
Proceedings of the Eighteenth International Conference on
Civil, Structural and Environmental Engineering Computing
Edited by: P. Iványi, J. Kruis and B.H.V. Topping
Civil-Comp Conferences, Volume 10, Paper 6.3
Civil-Comp Press, Edinburgh, United Kingdom, 2025
ISSN: 2753-3239, doi: 10.4203/ccc.10.6.3


# Numerical Investigation of Damage Identification in Historic Ceilings via Vibrations Measurements

**M. Chaabi[1], S. Mayfield[2] and P. Cacciola[3]**

**[1]School of Architecture, Technology and Engineering, University of Brighton, UK**
**[2]Senior National Conservator – Stone and Plaster, National Trust, United Kingdom**
**[3]College of Civil Engineering, Fuzhou University, China**

## Abstract

The sudden collapse of historic ceilings represents one of the major public safety issues threatening the heritage sector globally. The pressing need of fast, efficient and rigorous approaches to assess the health status of historic ceilings motivated the research presented in this paper. A stochastic approach is proposed as a tool to map the displacement response peak fractile at various locations of the ceiling, thus identifying any local anomalous deformation indicating critical areas within the ceiling. Extensive parametric studies on a FE model of a traditional plaster ceiling are undertaken to explore the potentiality of such approach.

**Keywords:** historic ceilings, health monitoring, damage detection, vibration measurement, environmental noise, random vibrations.

## 1 Introduction

Plaster ceilings were a common ceiling system for hundreds of years in the Americas, and for thousands of years in Europe [1]. The most common arrangement for a traditional ceiling is constructed by nailing riven timber laths up to timber ceiling joists. Materials tended to be vernacular (locally sourced) prior to nationwide and international distribution enabled by the railway network, so the materials used for a ceiling were chosen by the immediate resources around the site [2]. Lime plaster mixes with animal hair (horse, cow or goat) are the most commonly used for historic ceilings. Typically, the bed of laths of a traditional ceiling would have various undulations so the first coat of plaster (also known as backing, pricking up, or scratch

coat) would be applied to create the background. This coat would be spread across the laths, adhering to and pressing up through the gaps and forming the curling nibs (key) that, once set, mechanically tie the plasterwork to the structure [1,2]. This coat was then scratched with a splay of pointed laths to key the surface so that the next coat can lock into the face of the first. Once the plaster has carbonated and hardened enough (usually 4-14 days) the second coat, or float coat, made of the same mortar mix as the scratch coat, is applied to a smoother surface than the first. Another two to five days later the final face coat, or topcoat, of a finer 1:1 lime to a grained fine light sand is applied and trowelled to a fine, smooth face. Monitoring of traditional plaster ceilings has been effectively carried out for decades through visual and manual push tests. This method is, however, subjective with inherent obstacles due to logistics and costs of regular access required to the face and top side of the ceiling. The collapse of the ceiling at the Apollo Theatre, London, in 2013 drove the urgent need for survey methods that provide reliable empirical data. Causes of failures of plaster ceilings can be diverse ranging from vibrations at the floor above to water ingress, from notching of joists for installation of electrical or plumbing services to extreme changes in weight loading, however the age of a ceiling is often a primary risk factor [3]. In the present day a large portion of listed buildings have weak or vulnerable ceilings calling for innovative monitoring solutions. Many ceilings have no access above to inspect the condition of joists, laths and nibs. However, even with good access, visual inspection and human interpretation is the limit of current condition surveys which can easily miss hairline cracks. Inspection of the ceiling underside is foremost visual and tactile [4] aiming to identifying mainly cracks and detachments. On the other hand, remote survey methods, such as point cloud laser scanning and high-resolution photogrammetry, check levels of movement at each coplanar feature at up to ±3mm accuracy relative to an agreed horizontal datum level or previous scans [4].

In this regard a more rigorous, reliable and accurate approach might be sought in the field of System Identification and Damage Detection using vibration measurement see e.g. [5-11]. Moreover, the use of non-contact techniques is becoming more and more widespread in the field of the diagnostics of works of art and historical components. As an example, in [12] Laser Doppler Vibrometer (LDV) has been used to identify and characterise defects in frescoes, while in [13] the same technique has been used for the evaluation of the conservation state and restoration efficiency of nineteenth century Camorcanna vaults. Clearly, if the accessibility to the ceiling is granted as in [13] the technique Laser Doppler Vibrometer + Shaker is certainly promising. However, the electrodynamic shaker generally requires to be moved in various locations for large ceilings ensuring enough energy is introduced in the system but at the same time it will be necessary to be limited to avoid inducing potential damage induced by the forced vibrations. More recently in [14] a comparison between various input sources and measurement through both accelerometers and LDV on fibrous plaster ceilings has been presented, using a stochastic approach to determine relevant damage indicators. In this paper extensive numerical analyses on traditional plaster ceiling in which artificial damage is applied are undertaken. The stochastic approach originally proposed in [14] for fibrous plaster ceiling is herein extended to traditional ceilings, whose construction and therefore dynamic behaviour is sensibly different. Indoor environmental noise modelled as a Gaussian white noise process is used as

input source. Results confirm the proposed approach led to a clear identification of damage presence and position.

## 2 Methods

Consider the plaster ceiling modelled as a linear system undergoing support excitation. The equations governing the motion of the ceiling can be written in the frequency domain in the following form.

$$\left(\widetilde{\mathbf{K}} - \omega^2\mathbf{M}\right)\mathbf{U}(\omega) = \mathbf{K}\boldsymbol{\tau}U_s(\omega) \tag{1}$$

Where $\mathbf{U}(\omega)$ is the vector collecting the absolute displacements of the discretized ceiling, $\widetilde{\mathbf{K}}$ is the dynamic complex stiffness matrix, $\mathbf{M}$ is the mass matrix, $\boldsymbol{\tau}$ is the incidence vector and $\mathrm{U}_s(\omega)$ is the ceiling support (e.g. lateral walls, joists) movement induced by the indoor environmental noise, herein assumed as zero-mean gaussian stationary white noise random process. The stochastic response of the ceiling under the above hypothesis is fully defined by the knowledge of the power spectral density matrix, $\mathbf{S_U}(\omega)$, given by the following equation:

$$\mathbf{S_U}(\omega) = \mathbf{H}(\omega)\mathbf{H}^{\mathrm{T}}(\omega)\mathrm{S}_{\mathrm{U}_s} \tag{2}$$

Where $\mathbf{H}(\omega)$ is the transfer vector defined as

$$\mathbf{H}(\omega) = \left(\widetilde{\mathbf{K}} - \omega^2\mathbf{M}\right)^{-1}\mathbf{K}\boldsymbol{\tau} \tag{3}$$

While $\mathrm{S}_{\mathrm{U}_s}$ is the power spectral density function (assumed constant) of the indoor environmental noise. Once determined the response power spectral density function the peak displacement fractile of order $p$, $U_{j,max}(p,T)$, at a selected point "j" of the ceiling is given by the following equation

$$U_{j,max}(p,T) = \eta_{U_j}(p,T,\lambda_{0,U_j},\lambda_{1,U_j},\lambda_{2,U_j})\sqrt{\lambda_{0,U_j}} \tag{4}$$

in which $T$ is the time observing window, $\eta_{U_j}$ is the peak factor [15]

$$\eta_{U_j} = \sqrt{2\ln\left\{2N_{U_j}\left[1 - \exp\left[-\delta_{U_j}^{1.2}\sqrt{\pi\ln\left(2N_{U_j}\right)}\right]\right]\right\}} \tag{5}$$

with

$$N_{U_j} = \frac{T}{-2\pi\ln p}\sqrt{\frac{\lambda_{2,U_j}}{\lambda_{0,U_j}}} \tag{6}$$

and

$$\delta_{U_j} = \sqrt{1 - \frac{\lambda_{1,U_j}^2}{\lambda_{0,U_j}\lambda_{2,U_j}}} \tag{7}$$

where the response spectral moments $\lambda_{i,U_j}$ are given by the following equation:

$$\lambda_{i,U_j} = \int_0^{\infty} \omega^i G_{U_j}(\omega)\mathrm{d}\omega; \quad i=0,1,2 \tag{8}$$

where $G_{U_j}(\omega)$ $(= 2S_{U_j}(\omega), \forall\omega \geq 0; = 0, \forall\omega < 0)$ is the unilateral power spectral density function of the displacement $U_j$.

It has to be emphasized the power spectral density of the response can be determined experimentally from dynamic measurements either through an ensemble of recorded time histories by averaging their squared modulus of the Fourier Transform or (most common practice for environmental noise) by recording a time history long enough from which it is possible to extract a number of trajectories and then to average their squared Fourier Transforms up to convergency. Once the displacement peak fractiles are determined for several points of the ceiling they can be compared for a rapid estimation of possible local valleys so identifying weak areas, i.e. areas of the ceiling manifesting large displacements in comparison to the other points, likely due to damage.

## 3 Results

In this section the proposed strategy to identify potential damage in historic ceiling is scrutinized through a series of parametric tests. The numerical model depicted in Figure 1 is used for this purpose.

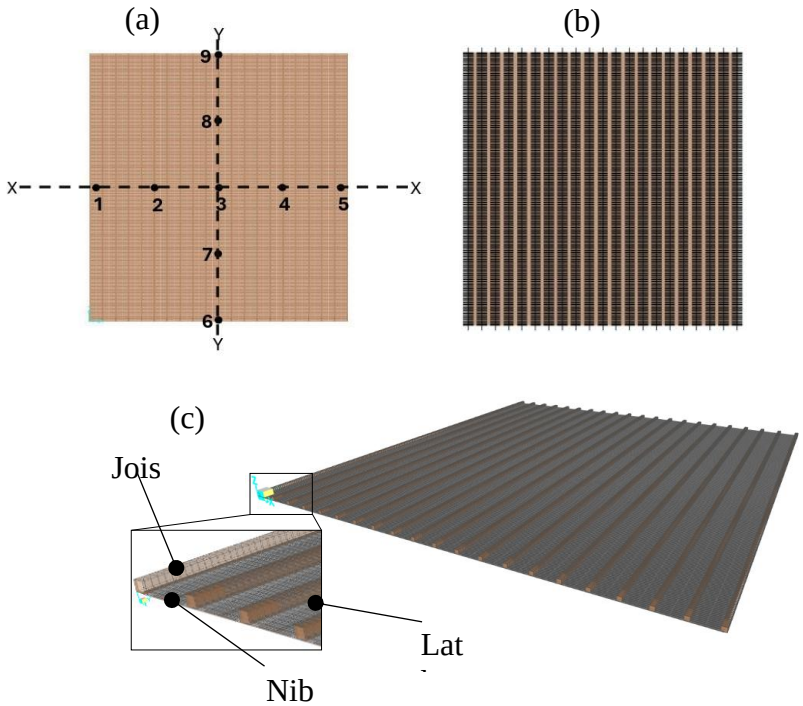


Figure 1. Numerical model of a traditional historic ceiling: a) Location of studied points in top view of the ceiling, b) Location of restraints, c) Structural components of the undamaged ceiling.

Shell elements have been used for the ceiling, while frame elements have been used for the joists, laths and nibs. The latter have been modelled defining an equivalent rectangular cross section for a portion of a strip. The upper joist is assumed restrained through hinges. Mechanical properties of the material used in the numerical model are reported in Table 1.

| Material | Modulus of Elasticity [N/m$^2$] | Density [kg/m$^3$] |
|---|---|---|
| Plaster ceiling | 2.65x10$^8$ [16] | 1300.44 |
| Timber frame | 8x10$^9$ | 500.17 |

Table 1: Mechanical parameters used in the FE model

Figure 2 shows the static deformation of the ceiling under its own self-weight. Static displacements at selected points (See Figure 1a) are shown in Figure 3. Clearly toward the center of the ceiling larger displacements are expected, and due to the joist direction as expected we observe larger difference in the X direction rather than on the Y direction.

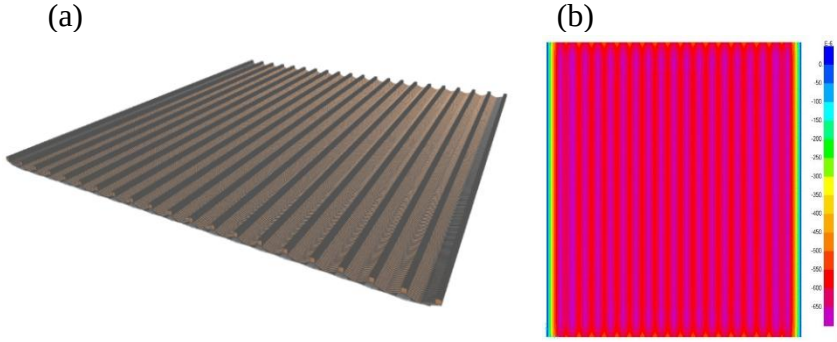


Figure 2. a) 3-D view of the deformed shape and b) contour map of the deformed shape of the undamaged ceiling under self-weight.

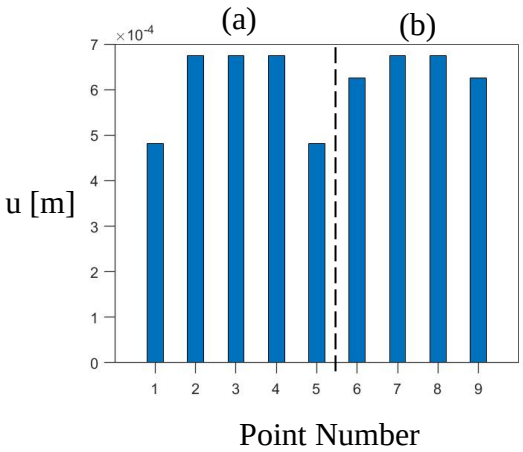


Figure 3. Static deformation under self-weight along a) central x-axis points, b) central y-axis points.

The dynamic behaviour of the model of the traditional ceiling is then explored. Joists are assumed fully fixed leading therefore to a rigid support structure and a deformable lath-ceiling system. The first five mode shapes of the undamaged ceiling are presented in Figure 4. The angular natural frequencies are practically identical although the mode shapes are sensibly different from each other. The modal participation factor, α, for each of them is also presented, showing very low contribution of the first three modes in the dynamic response of the ceiling, and 69% and 14% participation for the 4th and 5th mode, respectively.

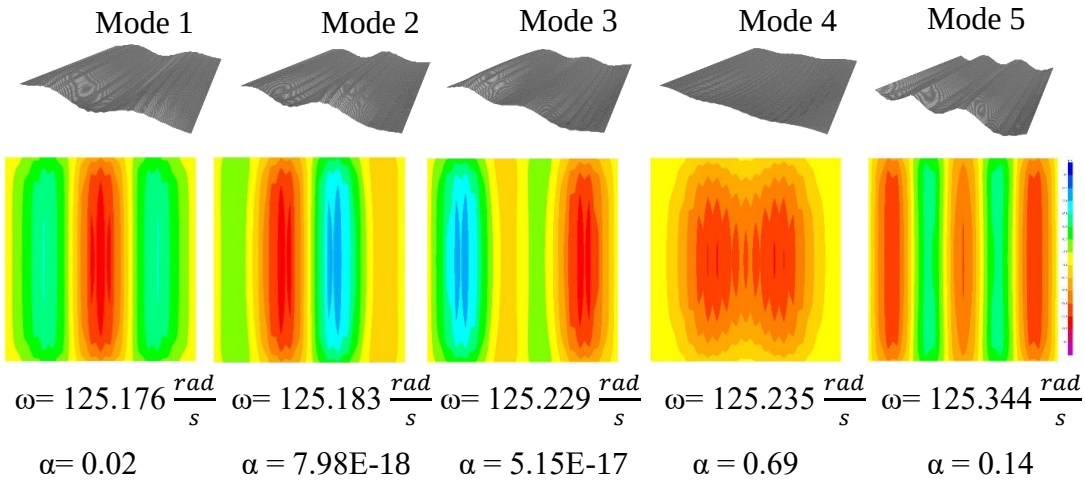


Figure 4. 3D view and contour maps of the first five mode shapes of the undamaged ceiling in z direction.

The ceiling has been then forced by clipped [0-200 rad/s] white noise uniform displacement process with $G_W = 2\ \frac{m^2}{s^3 rad}$ . The one-sided power spectral density of the relative displacement response of the selected points of the ceiling is given by the following equation:

$$G_{U_j}(\omega) = \left|H_j^2(\omega)\right| G_W \tag{10}$$

Where $\left|H_j^2(\omega)\right|$ is the modulus of the squared transfer function at the selected points. The calculated $G_{U_j}(\omega)$ for each point is plotted in Figure 5, showing, as expected, higher energy content in the response of points closer to the centre.

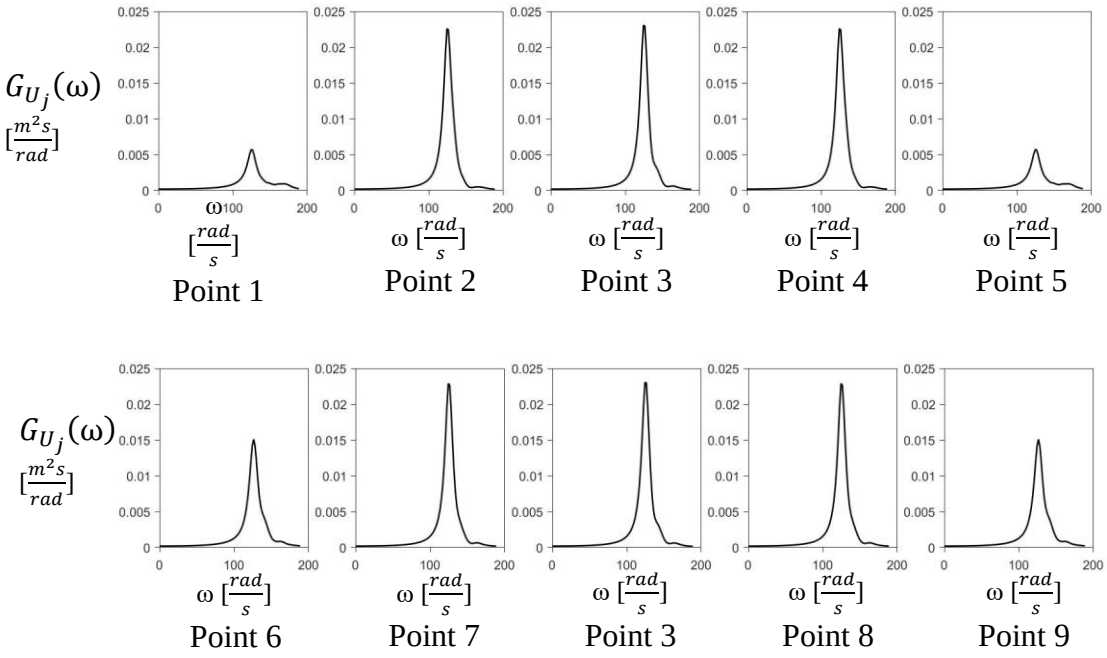


Figure 5. Power spectral density of the relative displacement response of the undamaged ceiling.

Artificial damage has been then introduced to the ceiling by deleting one or more nib strip connections starting at point 7 in the numerical model (see Figure 1). The 3-d view and z-direction contour map of the ceiling first mode under these progressive damage scenarios are shown in Figure 6, depicting a local mode around the damage location with a more evident valley on the damaged point, when the damage is more severe.

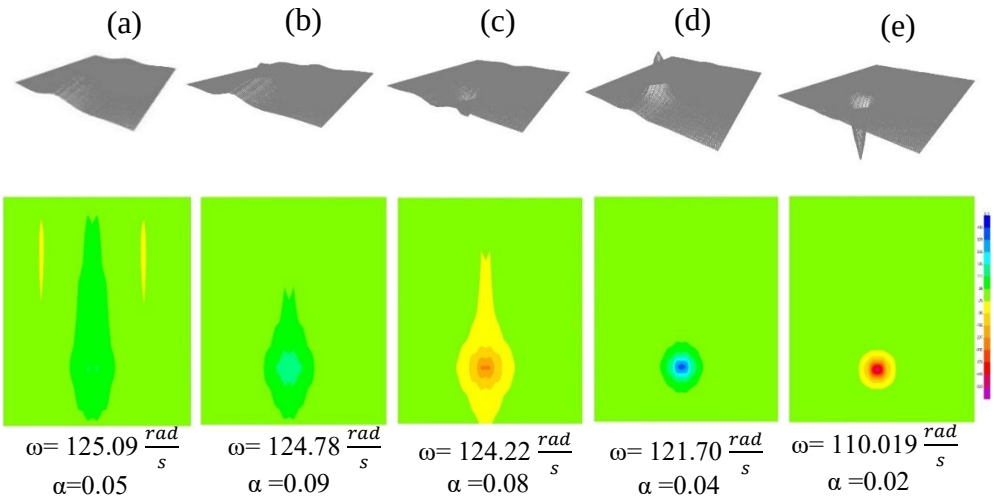


Figure 6. 3D view and contour maps of the first mode shape of the damaged ceiling in z direction in different damage scenarios: a) 1 broken nib, b) 2 broken nibs, c) 3 broken nibs, d) 5 broken nibs, and e) 10 broken nibs.

Interestingly, up to 5 broken nibs the pertinent modal frequency has a marginal reduction that will become more evident in the case of 10 broken nibs. The damage is also detectible in Figure 7, where the power spectral density of the undamaged and different damaged ceilings is plotted, showing a shift on the frequency of the peak on the damage location (point 7), as well as higher peaks for the larger damages. On the next step of the post-processing procedure of the response, the median peak displacement is calculated through equation 4, assuming a time observing window of 10 seconds. The expected peak responses are plotted in Figure 8, confirming previous information about the spatial variation of deformation across different points of the ceiling. Obviously, as a result of the symmetry of the structural components in the undamaged ceiling, the expected maximum displacement response is also symmetric.

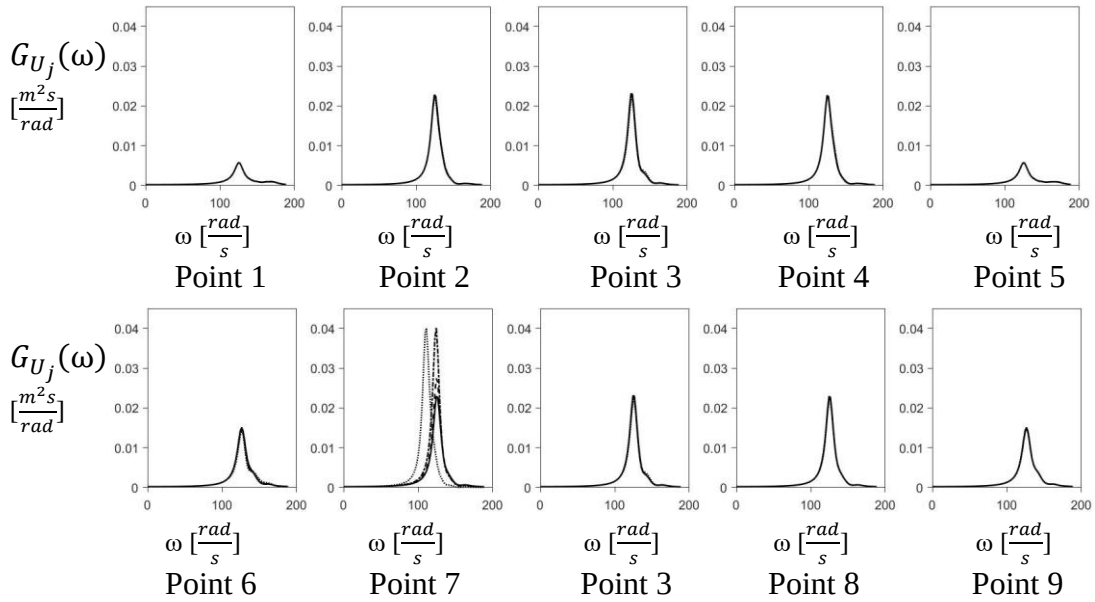


Figure 7. Power spectral density of the relative displacement response of the ceiling with different damage scenarios: solid line: undamaged, dashed line: one broken nib connection, dash-dotted line: three broken nib connection, and dotted line: ten broken nib connection.

The bar chart in Figure 8 shows the expected peak displacement fractile for the undamaged and for three different damaged cases, showing a jump in the response of the damage point. While the difference between the undamaged and the case with smallest damage (with only one broken nib connection) is small, it is still detectible. Considering other damage scenarios, the more severe the damage, the more pronounced the jump is in the maximum response at the damage location.

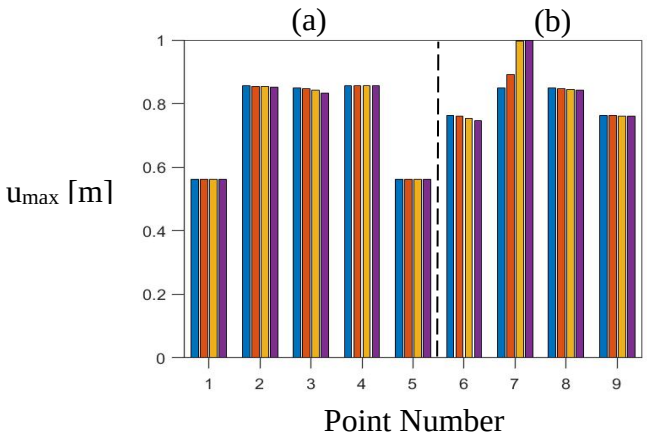


Figure 8. Normalized maximum expected relative displacement response of the ceiling under white noise excitation: a) central x-axis points, b) central y-axis points; Blue: undamaged, orange: one broken nib connection, yellow: three broken nib connection, and purple: ten broken nib connection

As transducers (accelerometers, Laser doppler vibrometer) measure absolute vibrations of the ceiling, the absolute displacement responses have been also used mimicking experimental data.

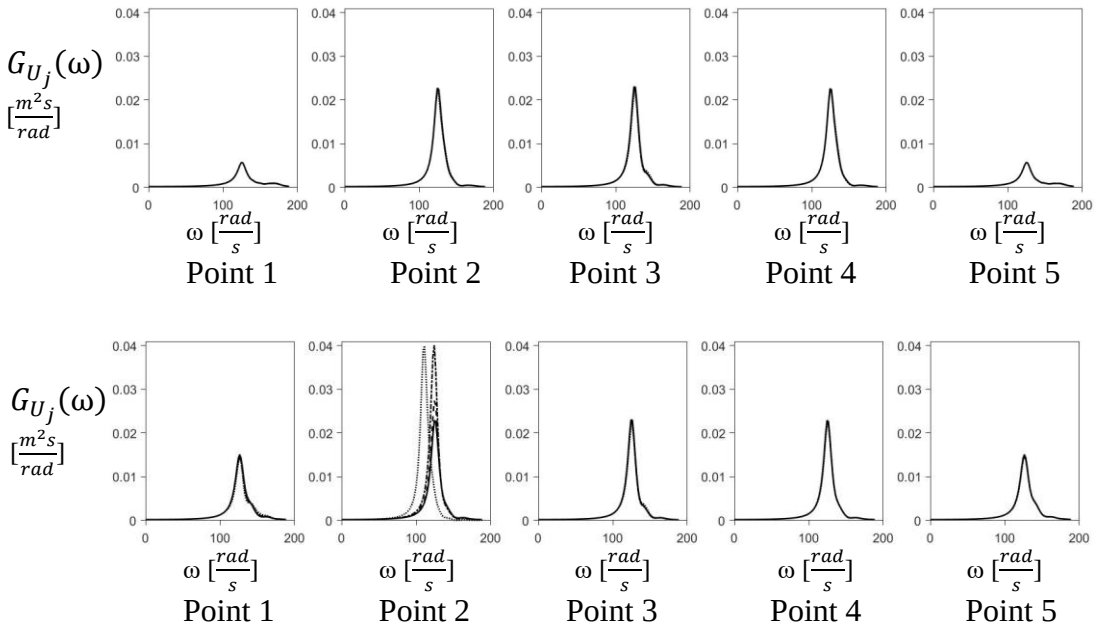


Figure 9. Power spectral density of the absolute displacement response of the ceiling with different damage scenarios: solid line: undamaged, dashed line: one broken nib connection, dash-dotted line: three broken nib connection, and dotted line: ten broken nib connection

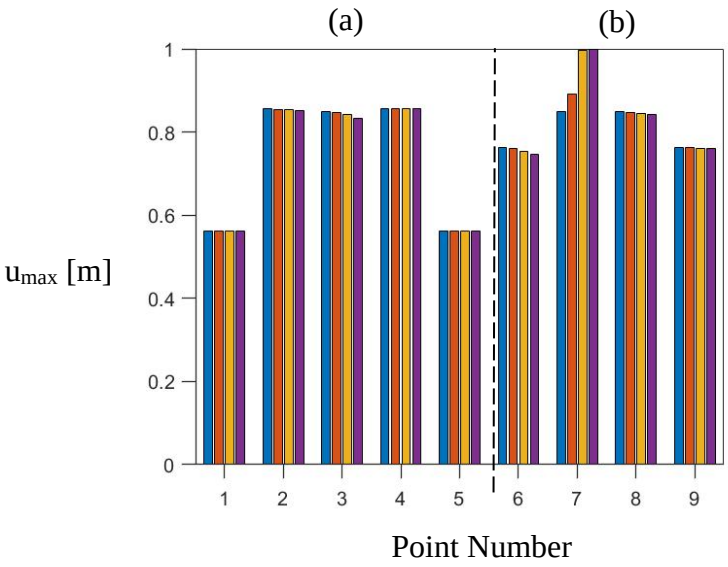


Figure 10. Normalized maximum expected absolute displacement response of the ceiling under white noise excitation: a) central x-axis points, b) central y-axis points; Blue: undamaged, orange: one broken nib connection, yellow: three broken nib connection, and purple: ten broken nib connection

As can be seen in Figures 9 and 10, the damaged cases have higher power spectral density peaks and higher expected maximum absolute displacement at the damage location, proving the practicality of the introduced method for damage detection and localization.

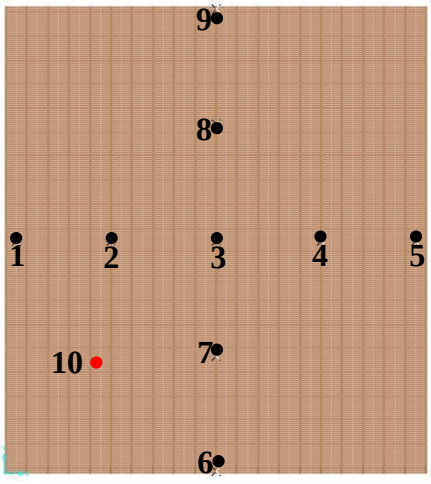


Figure 11. New damage location on point 10

Additional investigations have been undertaken considering a different location of the damage as indicated in Figure 11. Normalized maximum displacement are reported in Figure 12.

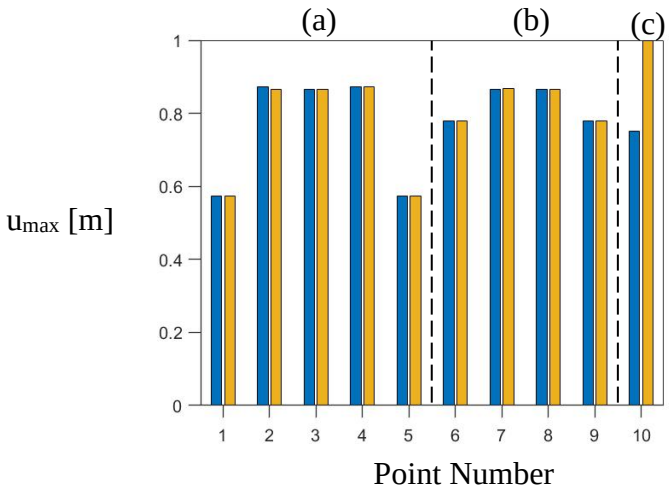


Figure 12. Normalized maximum expected absolute displacement response of the ceiling under white noise excitation: a) central x-axis points, b) central y-axis points, c) new damage location; Blue: undamaged, yellow: three broken nib connection.

Interestingly all the previous measurement points are practically unsensitive to the damage, while a clear high peak can be observed in the case in which a measurement points is taken in correspondence of the damage.

## 4 Conclusions and Contributions

In this paper extensive numerical tests have been undertaken for the study of damage identification in traditional historic ceilings. Basing on random vibration theory a novel damage identification strategy has been proposed. Specifically, fractiles of peak displacement has been used as damage indicators under the hypothesis of external input modelled as gaussian white noise process. Various damage scenarios have been considered as well as relative and absolute response parameters. In all the case the proposed approach has been proved to be successful to identify damage presence and location.

# References

[1] H. M. Currie, M. B. Bronski, and R. M. Lynde, "Stability Assessment of Historic Plaster Ceilings on Wood Lath", XV International Conference on Durability of Building Materials and Components DBMC, Barcelona C. Serrat, J.R. Casas and V. Gibert (Eds), 2020.

[2] S. Mayfield, "Best Practice Guide Repair of Historic Ceilings", Finishes and Interiors Sector Limited (FIS), 2024.

[3] S. Brookes, "Historic plaster ceilings. Part 1: Development and causes of failure", Struct. Eng. 99 (3), 20–24, 2021.

[4] S. Brookes, "Historic plaster ceilings. Part 2: Survey, assessment and methods of conservation", Struct. Eng. 99 (4), 30–33, 2021.

[5] S.W.Doebling, C.R.Farrar, M.B.Prime, D.W.Shevitz, "Damage Identification and Health Monitoring of Structural and Mechanical Systems from Changes in their Vibration Characteristics: A Literature Review", Los Alamos National Laboratory Report, LA-13070-VA5, 1996.
[6] S. Chesné, A. Deraemaeker, "Damage localization using transmissibility functions: a critical review", Mech. Syst. Signal Process. 38 (2), 569–584, 2013.
[7] O. Avci, O. Abdeljaber, S. Kiranyaz, M. Hussein, M. Gabbouj D. J. Inman, "A review of vibration-based damage detection in civil structures: From traditional methods to Machine Learning and Deep Learning applications", Mechanical Systems and Signal Processing 147, 107077, 2021.
[8] P. Cacciola, N. Impollonia, G. Muscolino, "Crack detection and location in a damaged beam vibrating under white noise", Computer and Structures, 81, 1773-1783, 2003.
[9] P. Cacciola, N. Maugeri, G. Muscolino, "Structural identification through the measure of deterministic and stochastic time-domain dynamic response", Computers and Structures, 89 (19-20), 1812-1819, 2011.
[10] S. Benfratello, P. Cacciola, N. Impollonia, A. Masnata, G. Muscolino, "Numerical and experimental verification of a technique for locating a fatigue crack on beams vibrating under Gaussian excitation", Engineering Fracture Mechanics, 74, 2992-3001, 2007.
[11] P. Cacciola, I. Calio', N. Fiorini, G. Occhipinti, D. Spina, A. Tombari, "Seismic response of nonlinear soil-structure interaction systems through the Preisach formalism: the Messina Bell Tower case study", Bulletin of Earthquake Engineering, 2021.
[12] P. Castellini, E. Esposito, V. Legoux, N. Paone, M. Stefanaggi, E.P. Tomasini, "On field validation of non-invasive laser scanning vibrometer measurement of damaged frescoes: experiments on large walls artificially aged". J. Cult. Herit. 1(2), S349–S356, https://doi.org/10.1016/S1296-2074(00)00145-X, 2000.
[13] A. Annessi, P. Castellini, E.O. Radaelli, L. Jurina, M. Martarelli, "Non-destructive Consolidation Assessment of Historical Camorcanna Ceilings by Scanning Laser Doppler Vibrometry". J Nondestruct Eval 39, 56, https://doi.org/10.1007/s10921-020-00701-5, 2020.
[14] P. Cacciola, RS. Mayfield, "Rapid screening of fibrous plaster ceilings health status using a laser Doppler vibrometer", Proceedings of the Institution of Civil Engineers -Engineering History and Heritage, ISSN 1757-9430 | E-ISSN 1757-9449, 2024.
[15] A. Der Kiureghian, "Structural response to stationary oscillation". J. Eng. Mech., 106(6): 1195–1213, 1980.
[16] C. Y. Rahimzadeh, A. S. Mohammed, A. A. Barzinjy, "Microstructure characterizations, thermal analysis, and compression stress–strain behavior of lime-based plaster", Construction and Building Materials, *350*, 128921, 2022.